Available online at www.sciencedirect.com

ScienceDirect

Procedia Structural Integrity 54 (2024) 91–98

Structural Integrity Procedia

www.elsevier.com/locate/procedia

International Conference on Structural Integrity 2023 (ICSI 2023)

Thermal analysis for testing underground battery location

E.S. Gonçalves[1], J. Gonçalves[2], H. Rosse[3], J. Costa[1], L. Jorge[1,4,5], J.A. Gonçalves[1,4,5], J.P. Coelho[1,4,5], J.E. Ribeiro[1,4,6*]

[1] *Instituto Politécnico de Bragança, 5300-052, Bragança; Portugal, * jribeiro@ipb.pt*
[2] *Valled, 5300-692, Bragança, Portugal*
[3] *MORE-Colab, 5300-358, Bragança, Portugal*
[4] *Laboratório Associado para a Sustentabilidade e Tecnologia em Regiões de Montanha (SusTEC), Campus Santa Apolónia, 5300-253 Bragança*
[5] *CeDRI— Research Centre in Digitalization and Intelligent Robotics, Campus Santa Apolónia, 5300-253 Bragança, Portuga*
[6] *CIMO—Mountain Research Center, Campus Santa Apolónia, 5300-253 Bragança, Portuga*

Abstract

The energy storage batteries, employed in solar systems installed on lampposts, are usually placed in devices such as switchboards fixed at an elevation near the top of the column. However, this storage solution becomes inefficient, because it is not possible to guarantee the control of the working temperature of the batteries, due to the low thermal insulation capacity of these storage devices. In this sense, an underground compartment made of concrete, steel plate and rock wool were created, embedded in the foundation of the lamppost, with the purpose of using geothermal energy to maintain an adequate temperature inside the compartment. To verify the temperature inside the battery storage compartment, a thermal analysis was performed, where heat transfer by conduction, convection and radiation was considered. Analyses were performed in steady state, and later, transient state, considering the initial temperatures of the thermal study in the previous steady state. With a storage volume of 1m3 and the base of the compartment at a depth of 2m, it was verified that it is possible to use geothermal energy to cool or heat, depending on the season, a system through geothermal energy. Considering a typical day in July, with room temperature of 35ºC, a reduction of approximately 8ºC was obtained inside the storage compartment, compared to the ambient temperature.

Keywords: Ambient temperature; Batteries; Thermal analysis;

* Corresponding author. Tel.: +0-351-273-303-081; fax: +0-351-273-303-000.
E-mail address: jribeiro@ipb.pt

10.1016/j.prostr.2024.01.060

1. Introduction

In the scope of energy efficiency, autonomous lampposts using photovoltaic panels and energy storage batteries have been installed. In this type of application, deep cycle batteries are normally used since most of their capacity are regularly used. Given their affordability, lead/gel batteries are a commonly used solution. Concerning installation, batteries are commonly placed in devices such as switchboards or inside the structure of lampposts, however, due to the low insulation capacity of the compartment, an adequate operating temperature cannot be guaranteed. In the case of lead/gel batteries, they can operate in more extreme temperature ranges, however the maximum useful life of these devices is only guaranteed by the producers at an ambient temperature of 25°C (Ultracell, 2022). High temperatures increase the capacity but decrease its lifetime, and low temperatures decrease its capacity (Vicent, 1997). In this context, several studies have been carried out on the influence of temperature variation in the charging and discharging processes, and on the useful life of batteries (Gencten, Dönmez and Şahin, 2016; Plangklang and Pornharuthai, 2013; Wang et al., 2022; Choi and Park, 2022). Several methods of controlling the operating temperature of the batteries have also been tested, namely through liquids or cooling gases (Jouharaa et al., 2022; Jilte and Kumar, 2018) or by creating a compartment with insulating materials to provide a stable operating ambient (Singh and Nguyen, 2022). With the studies already carried out, it is evident that extreme temperatures affect the life of batteries, causing premature aging, as well as impairing the performance since the capacity to charge and discharge is compromised (Hasan et al., 2017).

In this sense, within the VALLPASS project, this work aims to validate the installation of the batteries in an underground compartment, incorporated in the foundation of a lamppost, testing the possibility of using geothermal energy to maintain an adequate temperature for the operation of the batteries.

2. Methodology

2.1. Geothermal energy

Geothermal energy is an alternative and clean energy source already associated with numerous areas, including the climatization of buildings, electronic equipment, and agricultural greenhouses among other applications in which this energy source acts to provide favorable thermal conditions for the purpose in question. According to Calado (2016), through experimental measurements at various soil depths, he verified that due to the thermal inertia of the soil, there is a decrease in the thermal amplitude with advancement in depth. At deeper levels the soil presents a more stable thermal environment, exposing less significant temperature variations than those seen at depths closer to the surface which reveal a greater tendency to approach the thermal amplitudes felt in the outdoor environment, with higher diurnal and seasonal fluctuations.

Table 1 shows the measurements taken at the surface and at various depths at the site identified by Calado (2016) as "Site B" in his paper.

Table 1 – Annual temperature outside and at various depths

Profundity [m]	Temperature [°C]			
	Maximum	Minimum	Average	Thermal amplitude
Ambient temperature	29.4	9.7	18.3	19.7
1	22.9	9.0	15.0	13.9
2	20.6	11.2	15.1	9.4
3	19.5	12.8	15.5	6.7
4	18.4	13.5	15.8	4.9
5	18.9	14.7	16.3	4.2

2.2. Heat transfer

Heat transfer occurs when there is a temperature difference between two regions, and energy is exchanged from

the high temperature region to the lower temperature region through three modes of heat transfer:
- Conduction - a mode of heat transfer in which energy exchange takes place from the high temperature region to the lower temperature region by the kinetic motion or direct impact of molecules in the case of fluids at rest, or by the motion of electrons in the case of metals.
- Convection - mode of heat transfer between a surface and a moving fluid. The fluid can flow over a surface and heat transfer occurs if the temperature of the fluid is different from the temperature of the surface. In the case of natural or free convection, the fluid moves due to the rise caused by the density difference caused by the temperature difference of the fluid.
- Radiation - heat transfer process originated by the emission of electromagnetic radiation due to the temperature of the bodies. The bodies/surfaces besides emitting, can also receive and reflect radiation (Çengel, 2003).

Concerning heat transfer by radiation, the net rate of radiation heat transfer to a surface exposed to solar and atmospheric radiation is determined from an energy balance using the following formula (Çengel, 2003):

$$\dot{q}_{net,\ rad} = \alpha_s\, G_{solar} + \varepsilon\sigma\left(T_{sky}^4 - T_s^4\right) \tag{1}$$

where, $\dot{q}_{net,\ rad}$ is the net rate of heat transfer by radiation, in W/m^2, α_s is the radiation absorption coefficient, G_{solar} is the total incident solar energy, in W/m^2, ε corresponds to the emissivity of a surface, σ corresponds to the Stefan Boltzan constant equal to $5{,}670 * 10^{-8}\ [W/m^2 \cdot K^4]$, T_s represents the surface temperature in K, T_{sky} represents the atmospheric temperature, in K. The value of T_{sky} depends on the atmospheric conditions. It ranges from about 230 K for cold, clear-sky conditions to about 285 K for warm, cloudy-sky conditions.
The solar absorptivity α_s and the emissivity ε of some materials used in this study are shown in Table 2.

Table 2 - Comparison of the solar absorptivity α_s of some surfaces with their emissivity ε at room temperature (Çengel, 2003; Martinez, 2022).

Surface	Absorption coefficient (α)	Emissivity (ε)
Concrete	0,60	0,88
Granite	0,46	0,95
Carbon steel	0,20	0,2…0,6

To obtain the solar irradiance values, the "PVGIS tool" available in the Photovoltaic Geographic Information System was used, and direct, diffuse, and global solar irradiance values were obtained for each month, following the southward orientation and according to the inclination with respect to the horizontal plane of 0° in Table 3 and 90° in Table 4.

Table 3 – Annual variation of solar irradiance for a 0° angle in the city of Bragança (PVGIS, 2022)

Month	Jan.	Feb.	Mar.	Apr.	May	Jun.	Jul.	Aug.	Sep.	Oct.	Nov.	Dec.
Direct irradiance	175	285	362	405	530	602	718	656	514	313	200	169
Diffuse irradiance	139	164	207	247	244	240	193	184	191	175	146	130
Global irradiance	313	449	569	652	774	842	910	840	706	488	346	299

Table 4 – Annual variation of solar irradiance for a 90° angle in the city of Bragança (PVGIS, 2022)

Month	Jan.	Feb.	Mar.	Apr.	May	Jun.	Jul.	Aug.	Sep.	Oct.	Nov.	Dec.
Direct irradiance	332	400	345	249	222	203	269	384	408	376	349	359
Diffuse irradiance	117	136	148	151	137	129	109	118	139	140	125	120
Global irradiance	480	581	550	466	437	416	468	550	618	565	509	509

Regarding the heat transfer process by natural convection, the following steps were followed to obtain the free convection heat transfer coefficient for each exposed surface. Initially, the average temperature of the film generated between the surface and the convective air current was calculated using the expression (Çengel, 2003):

$$T_f = (T_s + T_\infty)/2 \tag{2}$$

where, T_f is the film temperature, T_s is de exposed surface temperature and T_∞ is the room temperature, all in K.

Subsequently, some air properties at different temperatures were obtained according to Table 5:

Table 5 - Air properties at atmospheric pressure (Incropera et al., 2017).

Surface temperature (T_s) [$°C$]	Ambient temperature (T_∞)[$°C$]	Film temperature (T_f) [K]	Kinematic viscosity (ν) [m^2/s] $*10^6$	Thermal conductivity (k) [$w/m.k$]	Prandtl number
0.0	-5.0	270.7	12.10	0.02391	0.00369
30.0	25.0	300.7	15.80	0.02629	0.00333
40.0	35.0	310.7	16.80	0.02705	0.00322

The properties shown in the previous Table were used to determine the Rayleigh number using the following equation (ÇENGEL, 2003):

$$Ra = \frac{g\beta(T_s - T\infty)L^3}{v^2}Pr \tag{3}$$

where, g is the gravitational acceleration in m/s^2, $\beta = \frac{1}{T_f}$ in k^{-1}, T_s is the surface temperature in K, T_∞ is the room temperature in K, L is the characteristic length in m, v is the kinematic viscosity in m^2/s and Pr is the Prandtl number.

Afterward, the calculation of the Nusselt number as well as the characteristic length varies according to the geometry of the surface and its arrangement, and these parameters are determined using the expressions shown in Table 6:

Table 6 – Empirical correlations for the average Nusselt number for natural convection over surfaces, adapted from (ÇENGEL, 2003).

Geometry	Characteristic length L_c	Range of Ra	Nu	
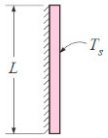	L	$10^4 - 10^9$	$Nu = 0{,}59Ra^{1/4}$	(4)
		$10^9 - 10^{13}$	$Nu = 0{,}1Ra^{1/3}$	(5)
		Entire range	$Nu = \left\{ \frac{0{,}387Ra^{\frac{1}{6}}}{\left[1 + \left(\frac{0.492}{Pr}\right)^{\frac{9}{16}}\right]^{\frac{8}{27}}} \right\}^2$ (Complex but more accurate)	(6)
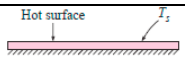	As/p	$10^4 - 10^7$	$Nu = 0{,}54Ra^{1/4}$	(7)
		$10^7 - 10^{11}$	$Nu = 0{,}15Ra^{1/3}$	(8)

Finally, the natural convection heat transfer coefficient was determined using the equation (ÇENGEL, 2003):

$$h = \frac{k}{L_c}Nu \tag{9}$$

where, h is the convective heat transfer coefficient in $w\ /\ m^2 \cdot K$, k is the thermal conductivity in $w/m \cdot K$, L_c is the characteristic length in m and N_u is the Nusselt number.

Regarding the process of heat transfer by conduction, it was not necessary to perform any calculations prior to the simulation, since, with the creation of the geometries for all constituent materials of the column-foundation assembly, including a soil control volume, it was only necessary to provide the properties of the constituent material of each component such as thermal conductivity and density.

Regarding soil properties, it is constituted of solid particles of different shapes and sizes and empty spaces occupied by air and water. Its thermal properties are therefore dependent on the water and air that fill its voids, and the different particles that constitute the solid phase (Lopes, Vieira and Soares, 2019). According to the work to determine the thermal conductivity of soil prepared by Lopes, Vieira and Soares (2019), it is verified that the

reference thermal conductivity for dry sandy soils is in the range between 0.3 $w/m \cdot K$ and 0.9 $w/m \cdot K$. These values are in agreement with the work of McCorry and Jones (2011) that present conductivity values for different types of soils and stones based on the German standard VDI 4640 (2010).
Thus, to consider the heat transfer by conduction, it was necessary to define the properties related to each constituent element of the column-foundation assembly, as summarized in Table 7:

Table 7 – Some properties of used materials (Santos and Matias, 2006)

Material	Density, ρ [kg/m^3]	Thermal conductivity, λ [W/(m.°C)]
Alloy steel	7700	50
Air	1.1	0.027
Rockwool	50	0.04
Granite	2500	2.8
Concrete	2300	1.65
Sandy soil	1330	0.6

2.3. Thermal analysis

In order to predict the temperature variation inside the battery storage compartment, SOLIDWORKS software was used to design and geometrically model a lighting column, as well as the different constituents that make up the foundation where the storage compartment is incorporated. This way the variations and heat transfers were calculated automatically through the creation of a control volume involving the various constituent materials of the post and foundation, including the air present inside both. Figure 1 shows on the left side a front view of the column-foundation assembly and on the right a cross section view of the assembly with the respective numbering and legend of the various constituent materials of the assembly.

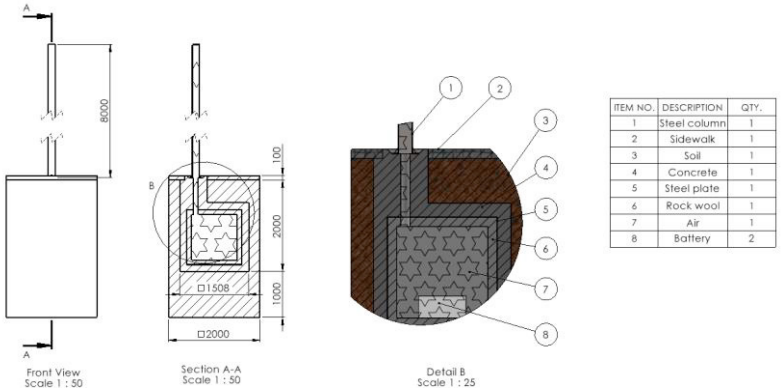

Fig. 1 – Column and foundation assembly

In Table 8 are presented the boundary conditions relative to the various heat transfer modes for each simulation. It was decided to analyze the temperature variation inside the foundation in three different months. Initially the month of January since this is when the minimum global irradiance occurs at a slope of 0° and has the lowest average annual temperatures. The month of July was also chosen because this month has the maximum global irradiance at a slope of 0° and is one of the hottest months of the year. Finally, the month of September was analyzed since it presents the maximum global irradiance at an inclination of 90°.
In each simulation the boundary conditions regarding the ground temperature were implemented and were obtained based on Table1. Also, to make each simulation more realistic, it was decided to place two batteries with dimensions typical of models found in the market, considering a heat generation relative to the charging and discharging processes of these equipment's, by defining these elements as heat sources.

Table 8 - Boundary conditions for each simulation

		Simulation 1 January ($T\infty = -5°C$)	Simulation 2 July ($T\infty = 35°C$)	Simulation 3 September ($T\infty = 25°C$)
Radiation	Une lateral surface of the column (global rad. at 90°)$[w/m^2]$	64.6	16.3	65.7
	Three lateral surfaces of the column (diffuse rad. at 90°) $[w/m^2]$	-8.0	-55.5	-30.1
	Column and flange top surface (global rad. at 0°) $[w/m^2]$	31.1	104.7	83.3
	Concrete surface (global rad. at 0°) $[w/m^2]$	49.7	205.8	168.9
	Sidewalk surface (global rad. at 0°) $[w/m^2]$	-5.1	51.4	49.9
Convection	Lateral surfaces of the column $[w/m^2K]$	2.6	2.2	2.3
	Flange surface $[w/m^2K]$	4.4	4.1	4.2
	Top surface of the column $[w/m^2K]$	5.0	4.6	4.7
	Concrete surface $[w/m^2K]$	4.0	3.7	3.7
	Sidewalk surface $[w/m^2K]$	2.7	2.5	2.5
Temperature at a depth of three meters $[°C]$		15.0	16.0	19.0
Temperature on the laterals of the soil control volume $[°C]$		6.0	24.0	21.0
Power dissipated by one battery* $[W]$		0.5	0.5	0.5

*For the calculation of the power dissipated, the Ultracell battery model UCG75-12 was considered, with an internal resistance of 6.6 mΩ. Admitting an operating voltage equal to 12V and an electric current requested equal to 8.75 A, a power dissipation of 0.5W per battery was obtained.

3. Results and Discussion

As already mentioned, the thermal conditions inside the battery storage compartment were analyzed in the months of January, July, and September, but due to space limitations only the heat transfer simulation images for July will be presented in this section. Still, the results for the three months are compared in the conclusions.

3.1. Temperature variation

Figure 2 shows the temperature variation inside the foundation on a typical day in July, where the maximum global solar irradiance is at 0°. In this analysis an ambient temperature of 35°C was considered.

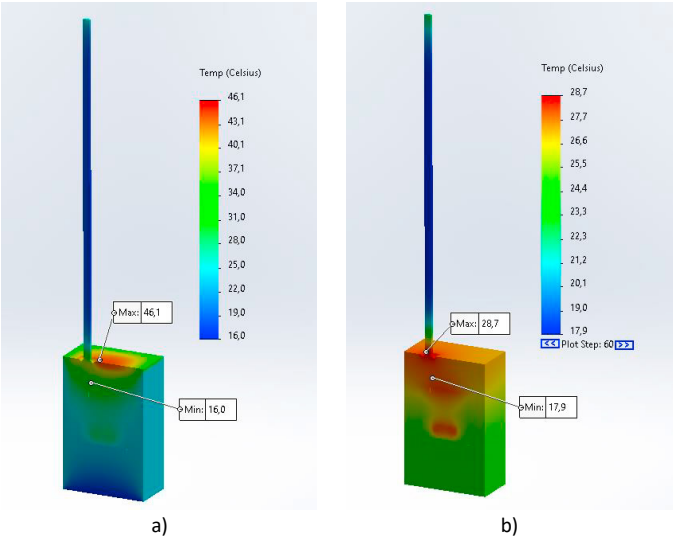

Fig. 2 - Temperature variation inside the foundation: a) steady state analysis; b) transient analysis after temperature stabilization (time=60min)

Through the graph in Figure 3 it is possible to observe the temperature variation over time inside the battery storage compartment, embedded in the foundation:

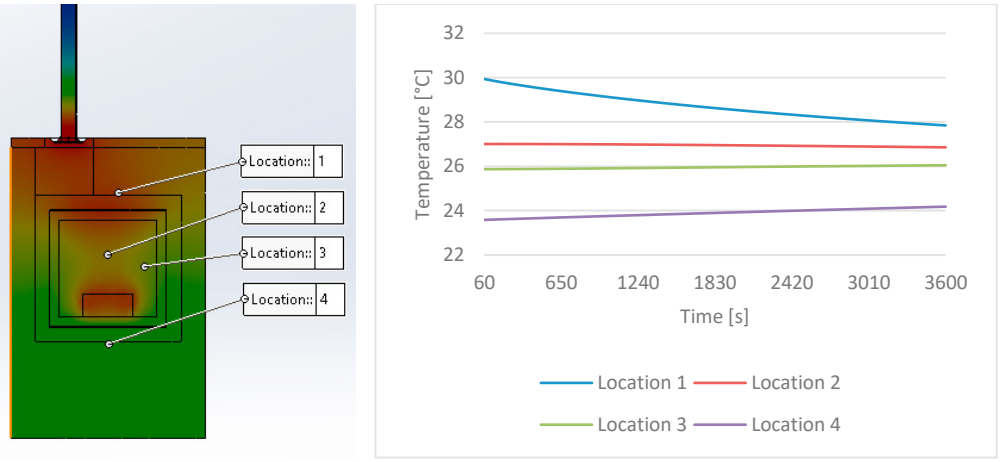

Fig. 3 - Temperature variation inside the battery storage compartment over one hour: a) location of the measurement points; b) temperature evolution

4. Conclusion

In summary, Table 9 shows the temperature values inside the storage compartment of the batteries, through the thermal analyses performed.

Table 9 – Results of the thermal analysis

Thermal analysis	S1	S3	S4
Month	January	Jun	September
Ambient temperature [°C]	-5,0	35,0	25,0
Temperature inside the compartment [°C]	6,0	27,0	23,0
Temperature variation [°C]	**+11,0**	**-8,0**	**-2,0**

With the values obtained, it was found that it is possible to use geothermal energy to cool or heat, depending on the season, a system through the soil. During the simulations it was verified that the performance of the battery storage compartment is influenced essentially by the depth, the thickness of the walls and the internal area.
In the analyses carried out, a depth of 3 meters was chosen, and it was verified that the depth of the compartment is a preponderant factor, since the soil presents a more stable thermal environment at higher depths, exposing less significant temperature variations than those verified at levels closer to the surface.
In the same sense, the thickness of the materials that constitute the battery storage compartment also influence the performance of the compartment, verifying that the increase in the thickness of the insulating material, contributed favorably to maintain a more stable operating environment and less susceptible to variations due to external environmental conditions. The insulating material chosen was rock wool with a thickness of one hundred millimeters.
Concerning the storage volume, a volume of $1m^3$ was used and it was found that that increasing the volume contributed favorably to maintaining a more stable environment inside the battery storage compartment.

Acknowledgements

The authors would like to thank the NORTE-01-0247-FEDER-113439 project for the financial support for this work. Part of financial support was also provided by Portugal's national funding FCT/MCTES (PIDDAC) to Centro de Investigação de Montanha (CIMO) (UIDB/00690/2020 and UIDP/00690/2020) andSusTEC (LA/P/0007/2020).

References

A. Calado. 2016. Monitorização da temperatura do solo. Desenvolvimento e estudo experimental de um permutador de calor ar-solo. Universidade da Beira Interior. http://hdl.handle.net/10400.6/7782

Anshuman Singh and Hung D. Nguyen. 2022. A two-layer framework for optimal control of battery temperature and microgrid operation. Journal of Energy Storage 50, 104057. https://doi.org/10.1016/j.est.2022.104057

A. G. Olabi, Hussein M. Maghrabie, Ohood Hameed Kadhim Adhari, Enas Taha Sayed, Bashria A. A. Yousef, Tareq Salameh, Mohammed Kamil and Mohammad Ali Abdelkareem. 2022. Battery thermal management systems: Recent progress and challenges. International Journal of Thermofluids 15, 100171. https://doi.org/10.1016/j.ijft.2022.100171

Boonyang Plangklang, Pornchai Pornharuthai. 2013. Mathematical Model and Experiment of Temperature Effect on Discharge of Lead-Acid Battery for PV Systems in Tropical Area. Energy and Power Engineering, 05(01). DOI: 10.4236/epe.2013.51006

C. A. Vicent. 1997. Modern Batteries- An Introduction to Electrochemical Power Sources, Second Edi. ISBN: 0-7506-7092-4

C. Santos & L. Matias. 2006. Coeficientes de Transmissão Térmica de Elementos da Envolvente dos Edifícios. Laboratório Nacional de Engenharia Civil.

F. P. Incropera, D. P. Dewitt, T. L. Bergman & A. S. Lavine. 2017. Principles of Heat and Mass Transfer. New York, United States: John Wiley & sons inc.

Henrique Lopes, Ana Vieira, Sofia Soares. 2019. Soil thermal behaviour: Characterization by the Hot Wire Method and numerical application. Geotecnia, 145. https://doi.org/10.24849/j.geot.2019.145.04

Hussam Jouharaa, Nicolas Sereya, Navid Khordehgaha, Robert Bennettb, Sulaiman Almahmouda and Stephen P. Lester. 2022. Investigation, development and experimental analyses of a heat pipe based battery thermal management system. International Journal of Thermofluids, 1-2, 100004. https://doi.org/10.1016/j.ijft.2019.100004

I. Martinez. 2022. PROPERTIES OF SOLIDS. http://imartinez.etsiae.upm.es/~isidoro/dat1/eLIQ.pdf

Jaehun Choi and Heesung Park. 2022. Correlation Between Changes in Environmental Temperature and Performance of High-Discharge Lithium-Polymer Batteries. Frontiers in Energy Research 10. https://doi.org/10.3389/fenrg.2022.830581

M. McCorry, G. Jones, (2011). Geotrainet Training Manual for Designers of Shallow Geothermal Systems. GEOTRAINET.

Md. Mehedi Hasan, Seyyed Ali Pourmousavi Kani, Feifei Bai and Tapan Kumar Saha. 2017. The impact of temperature on battery degradation for large-scale BESS in PV plant. Australasian Universities Power Engineering Conference (AUPEC). DOI:10.1109/AUPEC.2017.8282448

Metin Gencten, Koray Bahadır Dönmez, Yücel Şahin. 2016. Investigation of the temperature effect on electrochemical behaviors of TiO2 for gel type valve regulated lead-acid batteries. Applied Sciences and Engineering. https://doi.org/10.18038/aubtda.279856

R. D. Jilte, Ravinder Kumar. 2018. Numerical investigation on cooling performance of Li-ion battery thermal management system at high galvanostatic discharge. Engineering Science and Technology, an International Journal 21, 957-969. https://doi.org/10.1016/j.jestch.2018.07.015

Ultracell. 2022. UCG Solar – 12V. https://www.ultracell.co.uk/assets/pages/products-ucgseries-12v.html

VDI 4640 (2010) Thermal Use of the Underground. Part 1: Fundamentals, approvals, environmental aspect. VDI-Gessellschaft Energie und Umwelt (GEU).

Xingxing Wang,Yujie Zhang, Hongjun Ni, Shuaishuai Lv, Fubao Zhang,Yu Zhu, Yinnan Yuan and Yelin Deng. 2022. Influence of Different Ambient Temperatures on the Discharge Performance of Square Ternary Lithium-Ion Batteries. Energies 15, 5348. https://doi.org/10.3390/en15155348

Y. A. Çengel. 2003. Heat Transfer - A Pratical Approach. McGraw - Hill.